JACS
JOURNAL OF THE AMERICAN CHEMICAL SOCIETY

Article

pubs.acs.org/JACS

Surface-Enhanced Infrared Absorption Using Individual Cross Antennas Tailored to Chemical Moieties

Lisa V. Brown,[†,⊥] Ke Zhao,[‡,⊥] Nicholas King,[§,⊥] Heidar Sobhani,[‡,⊥] Peter Nordlander,*[,‡,§,⊥] and Naomi J. Halas*[,†,‡,§,⊥]

[†]Department of Chemistry, [‡]Department of Electrical and Computer Engineering, [§]Department of Physics and Astronomy, and [⊥]Laboratory for Nanophotonics, Rice University, Houston, Texas 77005, United States

Supporting Information

ABSTRACT: The development of antenna structures for surface-enhanced infrared absorption spectroscopy (SEIRA) is a topic of intense and growing interest for extending IR spectroscopy to zeptomolar quantities and ultimately to the single-molecule level. Here we show that strong infrared spectroscopic enhancements can be obtained from individual gold nanoantennas using conventional IR spectrometric sources. The antenna structure dimensions can be tuned to enhance the IR modes of specific chemical moieties. Simulations of the electric field intensity in the antenna junction region reveal a maximum SEIRA enhancement factor of more than 12 000. These findings open new opportunities for analyzing IR vibrations of exceptionally small quantities of molecules using widely accessible light sources.

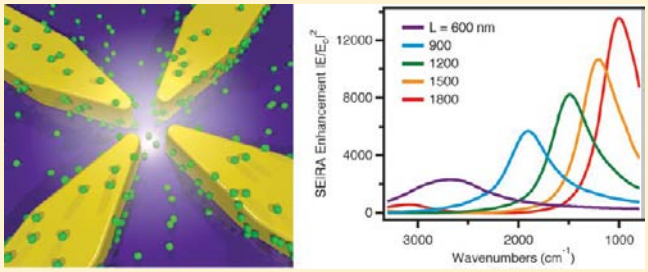

INTRODUCTION

Vibrational spectroscopy techniques provide important information concerning the structure, composition, and orientation of molecules. Infrared spectroscopy is one of the most universal methods for determining molecular composition and structure, where the "chemical fingerprints" of functional groups can be obtained by directly exciting dipole-active molecular vibrations with resonant IR light. There is currently an intense and growing interest in enhancing IR spectroscopy to obtain this level of vibrational information from extremely small quantities of molecules. Surface-enhanced infrared absorption (SEIRA) strategies have utilized metallic substrates, such as roughened or metal island films or, more recently, fabricated arrays of small metallic antennas, where molecules are located on or near the structure. The structures provide an intense, local, IR frequency field enhancement when illuminated and convey the resulting molecular response effectively to the far field, where it is detected. The enhancement of IR vibrational modes scales as $|E|^2$ of the local field.[1−5] Its better-known complement, surface-enhanced Raman scattering (SERS), has greatly benefited by this approach, which has resulted in single-molecule SERS sensitivities.[6−8] Since the selection rules of these two spectroscopies are complementary, there is a substantial motivation to enhance SEIRA to similar single-molecule or few-molecule sensitivity.

The strong local fields at illuminated metal structures responsible for SEIRA and SERS enhancements are due to excitation of the collective oscillations of the metal electrons of the structure, known as surface plasmons.[1,9] The size, shape, and composition of the metal structure determine its resonant frequencies, which can be tuned across specific frequency ranges of the electromagnetic spectrum.[10,11] If a metallic antenna structure has a plasmon resonance at the same frequency as a molecular vibration, the metal and molecule systems can couple, resulting in spectral features with Fano lineshapes[1,3,5,12,13] characteristic of a coupling between broad and narrow energy states.[14−21]

For SEIRA, simple antenna structures such as nanorods can provide enhanced IR vibrational signals;[3] however, a high-intensity tunable light source, such as a synchrotron, is then required for adequate signal intensity.[20,21] For conventional IR sources, large arrays of nanoscale antennas are required to provide a sufficiently strong signal for detection.[5,13]

An ideal solution for making SEIRA more widely accessible would be to create an antenna structure that can provide single-antenna hot-spot sensitivity using standard, widely available IR spectrometers and sources. In this study, we develop such an IR antenna and use it to detect zeptomolar quantities of molecules. The antenna has a cross geometry[22−24] consisting of four rods oriented at right angles with a small gap at the central junction. The inner tips of the rods are tapered to maximize local field enhancements and to reduce the gap spacing. This geometry enables efficient coupling of the antenna to unpolarized IR light. By varying the dimensions of the nanoantenna, it can be tuned to address and detect specific molecular vibrations. We demonstrate this property by tuning the antenna to the C−H stretches of an octadecanethiol self-assembled monolayer (SAM) and to the amide vibrations of hemoglobin. We also tune the antenna to the Si−O stretch of silica and use this

Received: December 30, 2012
Published: February 12, 2013

dx.doi.org/10.1021/ja312694g | J. Am. Chem. Soc. 2013, 135, 3688−3695

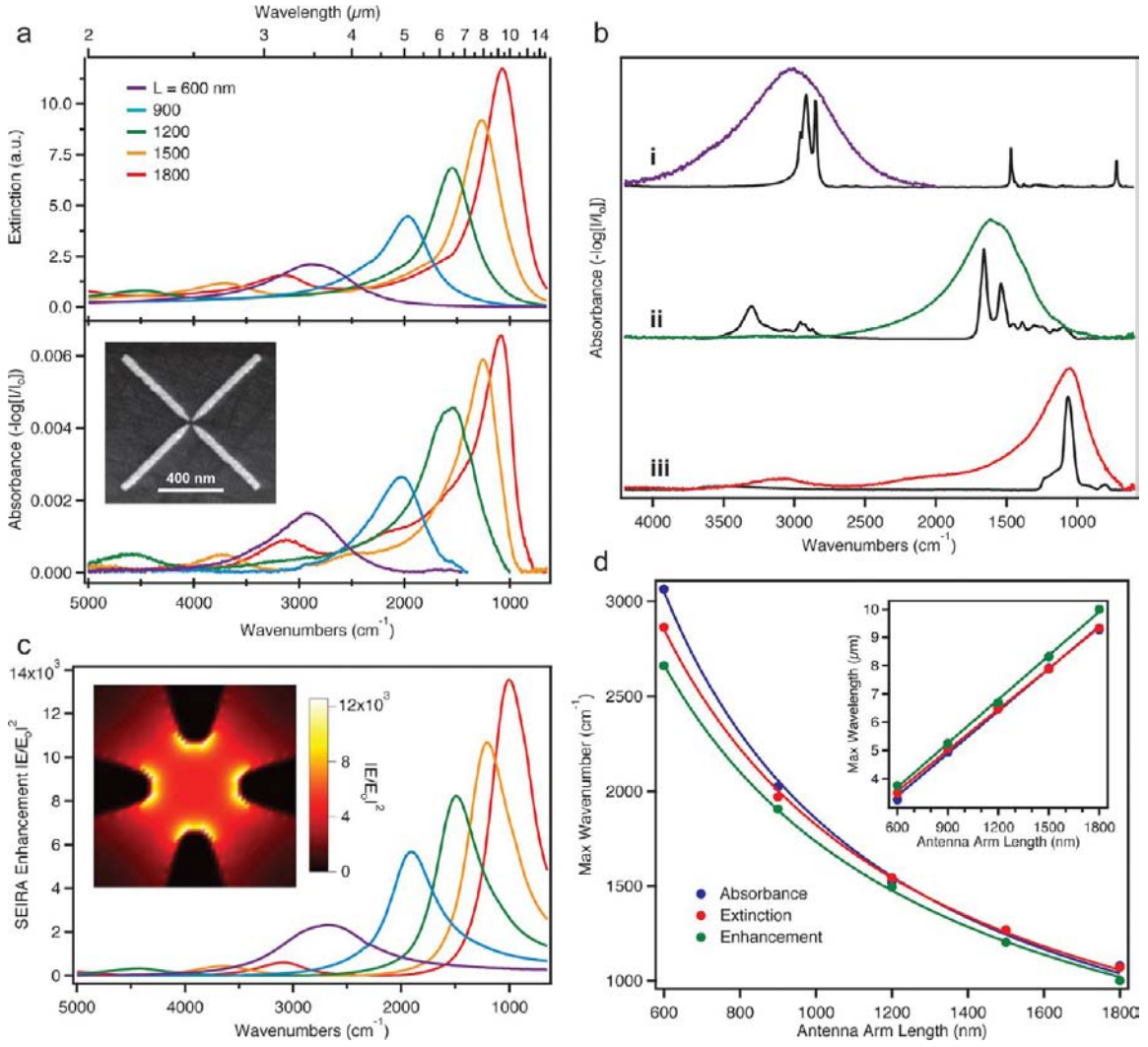

Figure 1. Properties of mid-infrared cross antennas. (a) Calculated (top) and measured (bottom) FTIR absorbance spectra of antennas with arm lengths L = 600−1800 nm. Inset: top view SEM image of antenna with L = 575 nm. (b) Bulk analyte spectra (black) and corresponding antenna spectra for ODT (i), Hb (ii), and silica (iii). Antennas have L = 575, 1200, and 1800 nm, respectively. Bulk spectra were obtained from a KBr pellet in (i) and ZnSe substrates in (ii) and (iii). (c) Theoretical SEIRA enhancement spectra ($|E/E_o|^2$) for antennas with L = 600−1800 nm. Spectrum colors match those in (a). Field intensities were taken from a point 2 nm away from one of the central tips. Inset: Map of SEIRA enhancement for L = 1200 nm at 1486 cm^{-1} over a 40 nm × 40 nm area in the junction region. (d) Wavenumber and wavelength (inset) for maximum absorbance (blue), extinction (red), and field enhancement (green) of the cross antenna as a function of L. Plots are fit to reciprocal and linear curves for wavenumber and wavelength, respectively.

vibrational mode to experimentally probe the enhancement properties of specifically selected regions of the antenna structure.

EXPERIMENTAL METHODS

Electron Beam Lithography. Gold cross antennas of several different sizes were prepared by electron beam lithography on ZnSe optical windows (12 × 1 mm, ISP Optics). Polymethyl methacrylate (PMMA A2, MicroChem) and Espacer 300Z (Showa Denko) were applied by spin-coating. Electron beam lithography was performed using an FEI Quanta 600 scanning electron microscope (SEM) with a beam voltage of 30 kV and a current of 40 pA. A 2-nm adhesion layer of titanium and a 35-nm layer of gold were deposited onto the samples by electron beam evaporation. The remaining PMMA was removed by incubation in *N*-methyl-2-pyrrolidone. Further details regarding the lithography procedure are given in the Supporting Information.

The antennas consist of four identical "arms" oriented at right angles. Each arm has a width of 50 nm and a total length L that ranges between 575 and 1800 nm. Toward the center of the antenna, the width tapers down to a tip with a curvature radius of 5−10 nm. The distance between opposing tips is approximately 35 nm.

Functionalization with Octadecanethiol (ODT). Antenna samples with L = 575 nm were placed in a 1-mM solution of ODT (Sigma Aldrich) in anhydrous ethanol at room temperature for >12 h. After incubation was complete, the samples were rinsed with ethanol and dried with nitrogen gas. A blank ZnSe sample underwent the same procedure to serve as a reference sample without antennas.

Functionalization with Hemoglobin (Hb). Lyophilized bovine Hb was obtained from Sigma Aldrich and dissolved in phosphate-buffered saline (Pierce) with 3 mM ethylenediaminetetraacetic acid (Sigma Aldrich) to a final concentration of 15 μM. Next, 5 mL of the protein solution was combined with 4 mL of 45.4 mM Traut's reagent (Pierce) and incubated for 1 h. This reaction converted primary amine groups to sulfhydryl groups for binding the proteins to the gold cross antennas. After the reaction was complete, excess Traut's reagent was removed using a Thermo Scientific Zeba Spin Desalting Column (Pierce).

Antenna samples with L = 1200 nm were placed in the solution at room temperature and incubated overnight. Afterward, the samples

dx.doi.org/10.1021/ja312694g | J. Am. Chem. Soc. 2013, 135, 3688−3695

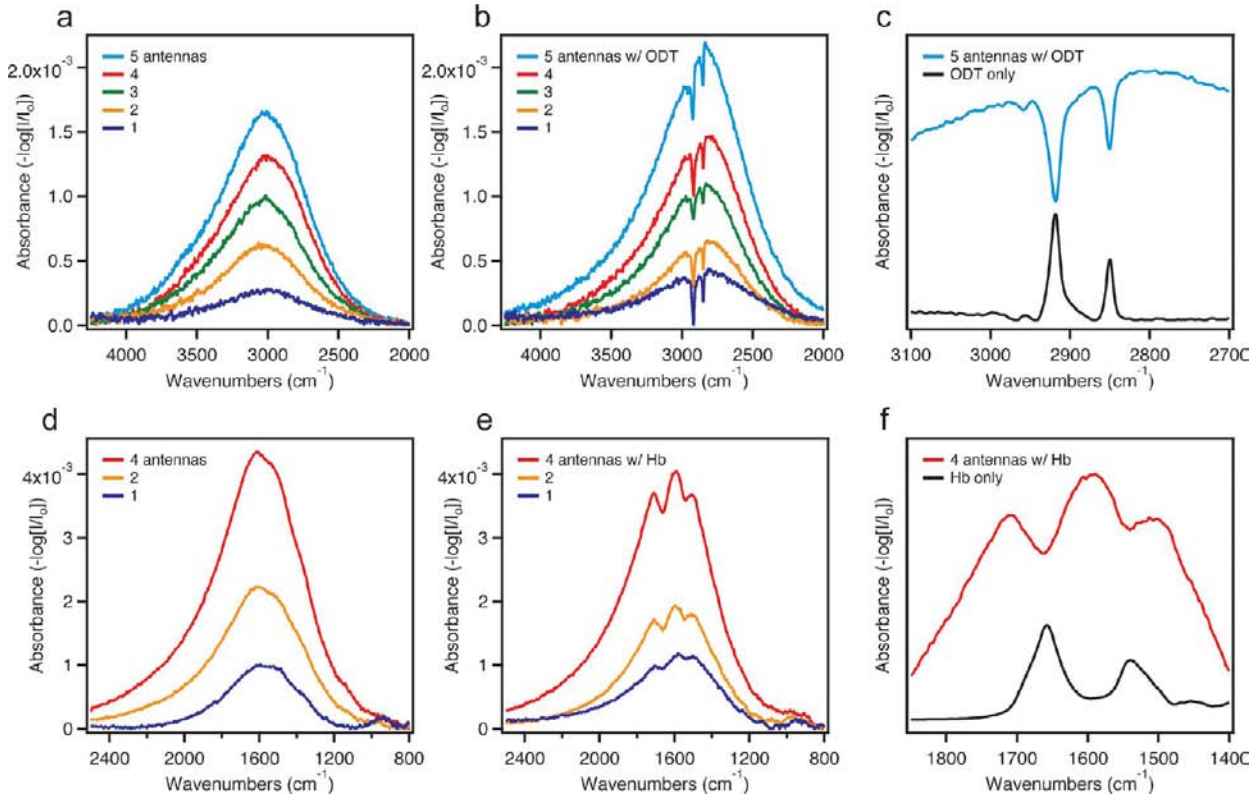

Figure 2. FTIR absorbance of octadecanethiol (ODT) and hemoglobin (Hb). (a) Cross antennas with L = 575 nm without ODT. (b) The same antennas as in (a) but with ODT. (c) Comparison of five antennas with ODT and a bulk spectrum of ODT obtained from a self-assembled monolayer on ZnSe. (d) Cross antennas with L = 1200 nm without Hb. (e) The same antennas as in (d) but with Hb. (f) Comparison between four antennas with Hb and a bulk spectrum of Hb obtained from a concentrated solution dried on ZnSe. (c) and (f) are scaled for clarity.

were rinsed with deionized water and dried with nitrogen gas. To prepare a reference sample without antennas, a concentrated solution of Hb was dropped onto a clean ZnSe substrate and let dry in air.

Silica Deposition. Antenna samples with L = 1800 nm were prepared using electron beam lithography as described above. Following this, a second lithography step was performed with PMMA A4 resist (MicroChem) and Espacer. After development, 2 nm of titanium and 50 nm of amorphous silica were deposited by electron beam evaporation. Deposition areas of silica over portions of antennas were circular with a radius of 150 nm. Deposition areas over entire antennas were circular with a radius of 3 μm.

Fourier Transform Infrared (FTIR) Spectroscopy. FTIR spectra were obtained using a Bruker Vertex 80v spectrometer and a Hyperion 3000 microscope. The instrument was equipped with a mercury–cadmium–telluride detector, a KBr beam splitter, and a globar light source. The mirror velocity was 20 kHz, and the spectral resolution was 4 cm^{-1}. Nearly all optics consisted of uncoated aluminum mirrors for extended ranges not used in this study. The spectrometer was purged under vacuum, and the microscope was purged with nitrogen gas for at least 3 h prior to analysis. To purge the microscope stage area, a Plexiglas housing was placed over the front of the microscope. Unpolarized light was used for all measurements. After the data were acquired, transmittance spectra were converted to absorbance, and a baseline correction was performed for each spectrum using the OPUS 6.5 software. Further details regarding the FTIR analyses are given in the Supporting Information.

Calculations. The finite difference time domain (FDTD) method (Lumerical Solutions software) was used to calculate extinction and near-field enhancement data for cross antennas on an infinitely large ZnSe substrate. The optical constants for the materials were taken from tabulated data.[25] The substrate was in the x–y plane, and the light wave was propagating in the positive z direction with circular polarization. The antenna geometry was the same as that described in the electron beam lithography fabrication, and the central tips of the antenna were rounded with a curvature radius of 6 nm. All near-field enhancement data were normalized to the electric field intensity transmitted through a bare ZnSe substrate.

The finite element method (FEM) was used to calculate extinction and field enhancement data in the far-infrared (FIR) and terahertz (THz) regimes. The antenna geometry was the same as that for the FDTD simulations, except with different L values and no substrate. The light source was linearly polarized parallel to one of the rod axes.

RESULTS AND DISCUSSION

Antennas for Several Analytes. By changing the arm length L, the resonance frequency of the cross antenna can be tuned across the IR region. In Figure 1a, we compare theoretical far-field extinction spectra (top) with measured FTIR absorbance spectra (bottom) for antennas with L ranging between 600 and 1800 nm. As L increases, the antenna resonance shifts to lower wavenumbers and increases in intensity. The inset shows a typical SEM image of a cross antenna with L = 575 nm. This was chosen so the antenna resonance would overlap with the C–H stretches of ODT (Figure 1b). Similarly, antennas with L = 1200 and 1800 nm were designed and fabricated to overlap with the amide bands of Hb and the Si–O phonon modes of silica, respectively.

Simulated SEIRA enhancements ($|E/E_o|^2$) for the antenna structures are shown in Figure 1c. In each simulation, the incident light was circularly polarized to model the unpolarized light used in the experimental measurements. The enhancement values were obtained in the antenna junction at a position 2 nm away from one of the antenna tips to avoid regions of the structure where quantum effects would reduce the induced electric fields.[26] As L increases, the maximum field enhance-

dx.doi.org/10.1021/ja312694g | J. Am. Chem. Soc. 2013, 135, 3688–3695

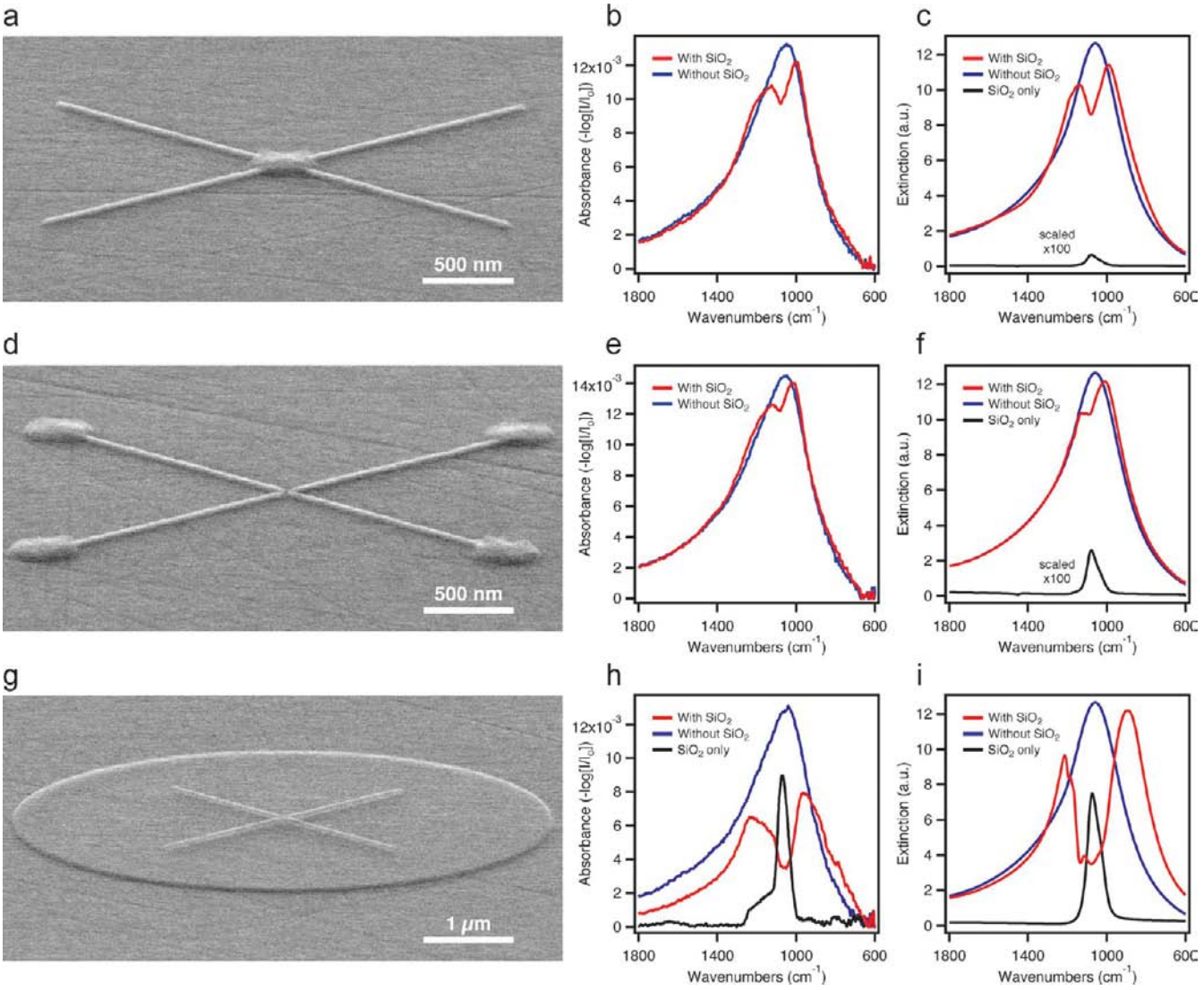

Figure 3. Spatial characterization of antennas using silica. (a,d,g) SEM images at a 75° tilt showing silica patches deposited in the junction (a), on the ends of the rods (d), and over the entire structure (g) for antennas with L = 1800 nm. (b,e,h) FTIR absorbance spectra for 3×3 arrays of antennas with silica (red) and without silica (blue) for the spatial arrangements shown in (a), (d), and (g), respectively. A spectrum of silica without antennas (black) is included in (h) but not in (b) and (c) because the signal intensity was too small to be measurable. (c,f,i) FDTD extinction spectra for antennas with silica (red) and without silica (blue) and for silica without antennas (black) for spatial arrangements shown in (a), (d), and (g), respectively. Silica spectra in (c) and (f) are scaled by a factor of 100. See Figure S3 for SEM images at a 0° tilt.

ment also increases from 50 to 120. The peaks are slightly red-shifted from the extinction spectra in Figure 1a, which is a universal phenomenon in finite plasmonic structures.[27] At lower energies, the enhancement does not reduce to zero but instead saturates at a constant value due to a phenomenon known as the "lightning-rod effect", which has been observed previously in systems relevant to SERS and SEIRA.[2,28]

The inset in Figure 1c shows a 2D map of the SEIRA enhancement in the junction of an antenna with L = 1200 nm. The largest enhancement is located near the tip of each arm. At a point 2 nm away from the tip, it is about 8200, and at the center of the junction, it is about 5200. Enhanced fields also exist at the opposite end of each arm (not shown) but are substantially smaller. All areas with field enhancements will contribute to vibrational signals of adsorbed molecules. Here, we focus on the areas near the tips to emphasize the highest possible enhancements that can be produced by these structures.

The highly tunable nature of the cross antennas is illustrated in Figure 1d, where we have plotted the wavenumbers and wavelengths for the maximal absorbance, extinction, and field enhancement as a function of L. These graphs can serve as a guide to determine the necessary antenna length needed for analyzing any specific molecular vibration of interest in the mid-infrared range.

Octadecanethiol Detection. First, SAMs of ODT were formed and examined using cross antennas with L = 575 nm. The metal structures were fabricated in patterns of one to five antennas, where the spacing between the antennas was 10−15 μm to avoid coupling. Figure 2a shows the FTIR absorbance spectra for bare antennas. The absorbance intensity increases linearly with the number of antennas in each pattern. After the sample was functionalized with ODT, the antenna peaks broadened, red-shifted, and increased in intensity (Figure 2b). This red-shift indicates a change in the dielectric environment

dx.doi.org/10.1021/ja312694g | J. Am. Chem. Soc. 2013, 135, 3688−3695

of the antennas,[11] and it confirms that ODT formed a uniform SAM.

The C−H stretch modes are clearly visible as sharp dips within the antenna peaks in the spectral region near 3000 cm^{-1} (Figure 2b). Even a single antenna produces an intense molecular IR signal that descends to the signal baseline. The modes of the analyte are identified in Figure 2c, in which a five-antenna spectrum is compared to a spectrum obtained from an ODT SAM on a blank ZnSe sample. Three modes are identified: the symmetric CH_2 stretch at 2850 cm^{-1}, the asymmetric CH_2 stretch at 2919 cm^{-1}, and the asymmetric CH_3 stretch at 2957 cm^{-1}. Detection of the CH_3 terminal group tests the sensitivity of the antennas, since there is only one CH_3 group for each molecule compared to 17 methylene groups. The peak positions and relative intensities of the molecular modes closely match those in the ODT spectrum as well as a previous study of alkanethiol monolayers on ZnSe.[29]

Additional measurements of similar antenna patterns showed random variations in the intensities of the vibrational modes (see Figure S1 in the Supporting Information). Such variations could be caused by subtle differences in the antenna junction geometries or by differences in the specific orientations of the ODT molecules with respect to the polarization of the enhanced near field (see Figure S2). Similar effects of orientation dependence have been discussed in SERS studies.[30,31] In either case, the Fano coupling could be stronger or weaker for different antennas, producing variations in signal intensity. Further investigation is necessary to accurately determine the cause of this phenomenon. However, the fact that we observe such differences in the signal is direct evidence that the experiment is probing only a relatively small number of molecules in the junction.

Hemoglobin Detection. Antennas with a length of 1200 nm were used to analyze the amide I and amide II vibrations of Hb. Figure 2d shows the absorbance spectra of one, two, and four antennas prior to attachment of the protein. As seen in the previous ODT example, there is a linear increase in the peak intensity according to the number of antennas.

After the sample was covered with Hb, the antenna resonance peaks did not show a noticeable shift or increase in intensity (Figure 2e). This indicates that the molecules were dispersed across the sample with sub-monolayer coverage. In each spectrum, the vibrational signals of the amide bonds appear as dips within the antenna peaks and, again, are clearly observable from the single-antenna pattern.

In contrast to the variations in signal intensity between different antennas observed for ODT, the intensities for Hb are more consistent. This observation suggests that the amide bonds experience consistent levels of near-field enhancement. Hemoglobin is significantly larger than ODT and may not bind as easily to the interstices of the junction, where antenna-to-antenna variations in field enhancement are most likely to occur. Also, unlike the uniform arrangement of the C−H bonds in the ODT SAM, the amide bonds within each Hb molecule have different orientations. This would reduce or eliminate variations in signal strength due to orientation dependence of the amide vibrational modes relative to the antenna arms. In Figure 2f, we compare a four-antenna spectrum to a separate measurement taken from a concentrated Hb solution drop-dried on ZnSe. The amide I and amide II modes are clearly identifiable in the antenna spectrum at 1662 and 1540 cm^{-1}, respectively. The linewidths are much broader than the C−H modes in Figure 2c because the amide groups not only vary in orientation but also are present within several different chemical environments in a Hb molecule.

Spatial Characterization Using Silica. Thus far, we have shown that single-antenna IR detection of ODT and Hb can be achieved. In both cases, the molecules were deposited over the entire sample. Since the antennas possess localized regions of near-field enhancement, the analyte signal intensity is likely to vary, depending on the location of the molecules on the structures.

To determine the spatial origin of the vibrational signals, we deposited silica patches in selected regions on the antennas and compared the FTIR signal intensity of the Si−O phonon modes for each area. Three different spatial arrangements of silica patches were examined: (1) in the junction of the antenna (Figure 3a), (2) at the four outer ends of the rods (Figure 3d), and (3) over the entire antenna (Figure 3g). Antennas with rod lengths of L = 1800 nm were chosen so the antenna plasmon peak overlapped with the Si−O modes around 1100 cm^{-1}. For each pattern, the silica patch layer was approximately 50 nm thick, and an identical pattern of silica was prepared on a blank area on the same sample to serve as a background measurement.

Figure 3a,d,g shows tilted SEM images of antennas with silica patches deposited in each specified region. The corresponding FTIR absorbance spectra (Figure 3b,e,h) and theoretical extinction spectra (Figure 3c,f,i) are given to the right of each image. The data include antennas without silica (blue), antennas with silica patches (red), and silica patches only (black). An experimental silica spectrum was not obtained for the first two cases because the quantity of silica in these patterns was too small.

The slight discrepancy in the lineshapes between the calculated silica spectra in Figure 3i and the measured spectra in Figure 3h is due to our simplified model for the silica permittivity which only includes the most prominent 1080 cm^{-1} phonon mode and not the lower intensity shoulder from the nearby other silica phonon modes.[32,33]

The thickness of the silica patch in the antenna junction and at the rod ends was reduced to 17 nm in the calculations to provide good agreement with the FTIR data. We suspect that this lower effective thickness was necessary to accommodate for experimental discrepancies in the thickness, density, disorder, and/or composition of the silica that may have occurred while depositing the material within such a small area. For the third case, with the large silica patch covering the entire antenna structure, a thickness of 50 nm provided good agreement between the experimental and theoretical data. Additional SEM images at higher magnification are given in Figure S3.

In the first case, where the silica patch is in the junction, the Si−O vibration is strongly enhanced compared to the spectrum of silica only, which has been scaled by 2 orders of magnitude (Figure 3c). In the second case, where the silica patches are located on the ends of the rods, the signal is less intense, and when the entire antenna is covered with silica, there is substantially more signal than in the previous two analyses.

The large increase in intensity for the third case is expected because the effective thickness of the silica layer here is more than twice as large as in the first two patterns. If we use simulations to examine the same spatial arrangements for a silica thickness of 17 nm in all three cases, the contribution from the junction to the Fano resonance is 45% of the result from covering the whole antenna (see Figures S4 and S5). The rod ends provide 20%, and the rest of the antenna is

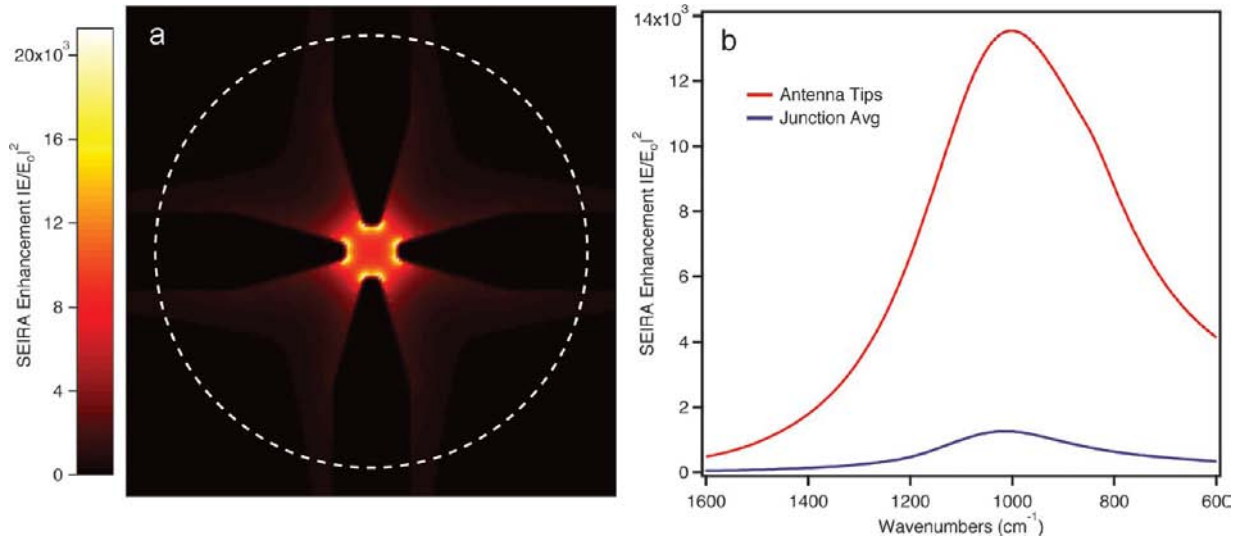

Figure 4. SEIRA enhancement factor. (a) Map of SEIRA enhancement ($|E/E_o|^2$) for a bare antenna with L = 1800 nm at 1080 cm^{-1} over an area of 170 nm × 170 nm in the junction region at a height of 17 nm above the substrate. The white dashed line indicates the area of integration for the blue curve in (b). (b) Comparison of SEIRA enhancement for a bare antenna with L = 1800 nm at a point 2 nm away from one of the central tips (red) and over a volume average of the area indicated in (a) with a height of 17 nm (blue). All data were obtained by FDTD calculations.

responsible for the remaining 35%. Additional simulations in which small areas of silica are placed on or within the vicinity of the middle of the rods show negligible signal (see Figure S6). These results clearly indicate that the Si−O vibrational signal predominantly originates from the junction with its large electric field enhancement.

SEIRA Enhancement. By comparing the Fano resonance intensity with the signal of the analyte in Figure 3c, we found that the junction area has a signal enhancement of approximately 750 (see Figure S7).

We also calculated $|E/E_o|^2$ factors to estimate the SEIRA enhancement.[4] Figure 4a shows the near-field enhancement (E/E_o) over a 170 nm × 170 nm area around the junction for a bare cross antenna with L = 1800 nm. The white dashed circle corresponds to the area covered by the silica layer in Figure 3c. By integrating $|E/E_o|^2$ over the volume of the silica patch, we obtained the average SEIRA enhancement as a function of excitation wavelength (Figure 4b, blue curve). At the peak absorbance of the silica phonon (1080 cm^{-1}), the enhancement is approximately 1100, which is similar to the signal enhancement of 750 mentioned above.

Much larger enhancement factors are found in the immediate area surrounding the tips of the antenna rods. The red curve in Figure 4b shows the SEIRA enhancement spectrum at a point 2 nm away from one of the antenna tips. The enhancement at 1080 cm^{-1} is about 12 000, and the peak enhancement value is about 13 500. To our knowledge, this is the highest reported theoretical SEIRA enhancement factor for the near-field intensity of a single-antenna structure.

Molecular Quantification. The high sensitivity of the present cross antennas to molecules in the junction demonstrated for silica patches is also expected to apply in the ODT and Hb measurements. By comparing the amount of space taken up by each molecule[6,34] with the total surface area used to define the regions of the junction and rod ends, 65% of the Fano resonance signal intensity for a single antenna accounts for about 5 amol of ODT and less than 40 zmol of Hb. Of this, nearly 70% comes from approximately 1 amol (560 000 molecules) and less than 10 zmol (5600 molecules) of ODT and Hb, respectively (see Supporting Information).

Far-Infrared and Terahertz Properties. Our antenna structures exhibit even stronger enhancements in the FIR and THz regimes. Figure 5a shows extinction spectra calculated by the FEM for cross antennas with lengths ranging from 600 nm to 13 μm. As the length increases, the extinction intensity continues to increase monotonically. An antenna with L = 13 μm has an extinction nearly 2 orders of magnitude larger than that for an antenna with L = 600 nm. The near-field enhancement also increases up to a factor of about 800 for L = 13 μm (Figure 5b), which corresponds to a SEIRA enhancement of more than 10^5.

As in Figure 1, the enhancement spectra do not reduce to zero but saturate at a constant values due to the lightning-rod effect.[2,28] For a perfect metal, the lightning-rod enhancement is $(2L + D)/D$ and is shown with dashed lines in Figure 5b. At longer wavelengths, the antenna spectra have slightly lower intensity because the structures are composed of gold, which is an imperfect conductor.

The broad field enhancement from the lightning-rod effect is highly advantageous for spectroscopic studies since the signal is enhanced across the entire spectrum rather than for just a short range of frequencies. The cross antenna structure presented here should therefore also be useful for vibrational and rotational spectroscopy in the FIR and THz ranges.[35−37]

■ CONCLUSIONS

We have shown that individual cross antennas illuminated with a conventional IR source can be used for high-sensitivity SEIRA spectroscopy. The antennas can be straightforwardly tuned to overlap vibrational modes within a broad spectral range from the near-IR into the terahertz regimes. With this approach, we observed both the C−H stretching modes of octadecanethiol in a self-assembled monolayer around the antenna and also the amide vibrational modes of hemoglobin in the mid-IR spectral range. By combining controlled deposition of silica dots on selected positions of the antenna and SEIRA measurements of a silica vibrational mode, we show that the SEIRA signal

dx.doi.org/10.1021/ja312694g | J. Am. Chem. Soc. 2013, 135, 3688−3695

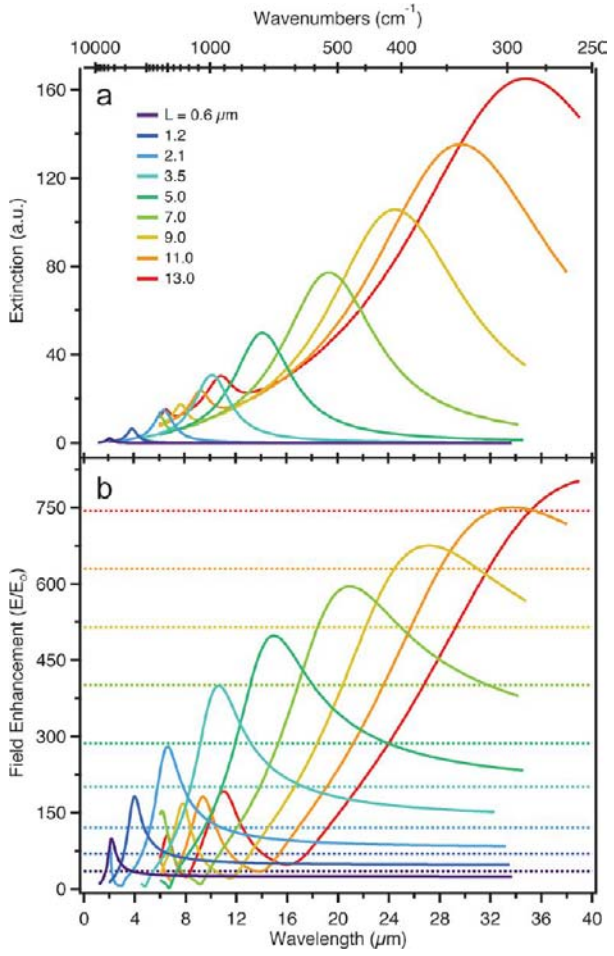

Figure 5. Far-infrared and terahertz properties. (a) Extinction spectra for antennas with L = 0.6–13 μm. (b) Field enhancement spectra for the same antennas as in (a) taken from a point 2 nm away from one of the central tips. Dashed lines represent $(2L + D)/D$, which corresponds to the enhancement from the lightning-rod effect for perfect conductors. All data were obtained by FEM calculations.

predominantly originates from molecules within a small junction at the center of the antenna. The predicted SEIRA enhancement factors for our structures are 4 orders of magnitude but are expected to become even larger in the far-IR and THz regimes. Further studies to extend the sensitivity of this approach are currently underway.

■ ASSOCIATED CONTENT

Supporting Information

Experimental methods, ODT signal variation, polarized near-field simulations, high-magnification SEM images, derivation of signal enhancement ratio, and quantification of ODT and Hb. This material is available free of charge via the Internet at http://pubs.acs.org.

■ AUTHOR INFORMATION

Corresponding Author

nordland@rice.edu; halas@rice.edu

Notes

The authors declare no competing financial interest.

■ ACKNOWLEDGMENTS

This work was supported by the Robert A. Welch Foundation (C-1220 and C-1222), Air Force Office of Scientific Research (AFOSR) FA9550-10-1-0469, the National Science Foundation Major Research Instrumentation (MRI) grant ECCS-1040478, the Defense Threat Reduction Agency (DTRA) HDTRA1-11-1-0040, the National Security Science and Engineering Faculty Fellowship (NSSEFF) N00244-09-1-0067, and the Army Research Office (MURI). We also thank Yang Li, Yumin Wang, Sandra Bishnoi, Ciceron Ayala-Orozco, Mark Knight, and Karl Gregory for helpful discussions.

■ REFERENCES

(1) Chen, K.; Adato, R.; Altug, H. *ACS Nano* **2012**, *6*, 7998–8006.
(2) Le, F.; Brandl, D. W.; Urzhumov, Y. A.; Wang, H.; Kundu, J.; Halas, N. J.; Aizpurua, J.; Nordlander, P. *ACS Nano* **2008**, *2*, 707–718.
(3) Neubrech, F.; Pucci, A.; Cornelius, T. W.; Karim, S.; Garcia-Etxarri, A.; Aizpurua, J. *Phys. Rev. Lett.* **2008**, *101*, 157403.
(4) Osawa, M. In *Near-Field Optics and Surface Plasmon Polaritons*; Kawata, S., Ed.; Topics in Applied Physics *81*; Verlag: Berlin/Heidelberg, 2001; pp 163–187.
(5) Pucci, A.; Neubrech, F.; Weber, D.; Hong, S.; Toury, T.; de La Chapelle, M. L. *Phys. Status Solidi B* **2010**, *247*, 2071–2074.
(6) Xu, H.; Bjerneld, E.; Kall, M.; Borjesson, L. *Phys. Rev. Lett.* **1999**, *83*, 4357–4360.
(7) Willets, K. A.; Stranahan, S. M.; Weber, M. L. *J. Phys. Chem. Lett.* **2012**, *3*, 1286–1294.
(8) Kneipp, J.; Kneipp, H.; Kneipp, K. *Chem. Soc. Rev.* **2008**, *37*, 1052–1060.
(9) Dadosh, T.; Sperling, J.; Bryant, G. W.; Breslow, R.; Shegai, T.; Dyshel, M.; Haran, G.; Bar-Joseph, I. *ACS Nano* **2009**, *3*, 1988–1994.
(10) Chen, H.; Kou, X.; Yang, Z.; Ni, W.; Wang, J. *Langmuir* **2008**, *24*, 5233–5237.
(11) Kelly, K.; Coronado, E.; Zhao, L.; Schatz, G. *J. Phys. Chem. B* **2003**, *107*, 668–677.
(12) Giannini, V.; Francescato, Y.; Amrania, H.; Phillips, C. C.; Maier, S. A. *Nano Lett.* **2011**, *11*, 2835–2840.
(13) Liberman, V.; Adato, R.; Mertiri, A.; Yanik, A. A.; Chen, K.; Jeys, T. H.; Erramilli, S.; Altug, H. *Opt. Exp.* **2011**, *19*, 11202–11212.
(14) Fano, U. *Phys. Rev.* **1961**, *124*, 1866–1878.
(15) Miroshnichenko, A.; Flach, S.; Kivshar, Y. *Rev. Mod. Phys.* **2010**, *82*, 2257–2298.
(16) Satpathy, S.; Roy, A.; Mohapatra, A. *Eur. J. Phys.* **2012**, *33*, 863–871.
(17) Lu, W.-T.; Wang, S.-J.; Li, W.; Wang, Y.-L.; Ye, C.-Z.; Jiang, H. *J. Appl. Phys.* **2012**, *111*, 103717.
(18) Cheng, M.-T.; Song, Y.-Y. *Opt. Exp.* **2012**, *37*, 978–980.
(19) Liu, S.-D.; Yang, Z.; Liu, R.-P.; Li, X.-Y. *ACS Nano* **2012**, *6*, 6260–6271.
(20) Xu, X. G.; Rang, M.; Craig, I. M.; Raschke, M. B. *J. Phys. Chem. Lett.* **2012**, *3*, 1836–1841.
(21) Huth, F.; Govyadinov, A.; Amarie, S.; Nuansing, W.; Keilmann, F.; Hillenbrand, R. *Nano Lett.* **2012**, *12*, 3973–3978.
(22) Biagioni, P.; Huang, J. S.; Duò, L.; Finazzi, M.; Hecht, B. *Phys. Rev. Lett.* **2009**, *102*, 256801.
(23) Unlü, E. S.; Tok, R. U.; Sendur, K. *Opt. Exp.* **2011**, *19*, 1000–1006.
(24) Gao, Z.; Wang, Z. Y. *J. Electromagnet. Wave* **2011**, *25*, 1730–1739.
(25) Palik, E. D. *Handbook of Optical Constants*; Academic Press: San Diego, 1998.
(26) Zuloaga, J.; Prodan, E.; Nordlander, P. *ACS Nano* **2010**, *4*, 5269–5276.
(27) Zuloaga, J.; Nordlander, P. *Nano Lett.* **2011**, *11*, 1280–1283.
(28) Liao, P. F.; Wokaun, A. *J. Chem. Phys.* **1982**, *76*, 751–752.
(29) Noble-Luginbuhl, A. R.; Nuzzo, R. G. *Langmuir* **2001**, *17*, 3937–3944.

(30) Creighton, J. A. *Surf. Sci.* **1983**, *124*, 209−219.
(31) Moskovits, M. *J. Chem. Phys.* **1982**, *77*, 4408−4416.
(32) Han, S.; Aydil, E. *Appl. Phys. Lett.* **1997**, *70*, 3269−3271.
(33) Velde, B.; Couty, R. *J. Non-Cryst. Solids* **1987**, *94*, 238−250.
(34) Ulman, A. *Chem. Rev.* **1996**, *96*, 1533−1554.
(35) Phillips, D.; Tanner, E.; De Lucia, F.; Everitt, H. *Phys. Rev. A* **2012**, *85*, 052507.
(36) Drouin, B. J.; Yu, S.; Pearson, J. C.; Gupta, H. *J. Mol. Struct.* **2011**, *1006*, 2−12.
(37) Martin-Drumel, M. A.; Pirali, O.; Balcon, D.; Bréchignac, P.; Roy, P.; Vervloet, M. *Rev. Sci. Instrum.* **2011**, *82*, 113106.